arXiv:0704.3510v2 [cond-mat.str-el] 2 Jul 2007

Coupling of phonons and spin waves in triangular antiferromagnet

Jung Hoon Kim[1] and Jung Hoon Han[1, 2, *]
[1]*Department of Physics, BK21 Physics Research Division,*
Sungkyunkwan University, Suwon 440-746, Korea
[2]*CSCMR, Seoul National University, Seoul 151-747, Korea*

We investigate the influence of the spin-phonon coupling in the triangular antiferromagnet where the coupling is of the exchange-striction type. The magnon dispersion is shown to be modified significantly at wave vector $(2\pi, 0)$ and its symmetry-related points, exhibiting a roton-like minimum and an eventual instability in the dispersion. Various correlation functions such as equal-time phonon correlation, spin-spin correlation, and local magnetization are calculated in the presence of the coupling.

PACS numbers: 75.80.+q, 71.70.Ej, 77.80.-e

I. INTRODUCTION

A number of recent experimental breakthroughs has revived interest in the phenomena of coupling between magnetic and electric (dipolar) degrees of freedom in a class of materials known as "multiferroics"[1]. Some noteworthy observations include the development of dipole moments accompanying the helical spin ordering[2,3], displacement of magnetic ions at the onset of magnetic order in the triangular lattice $YMnO_3$[4], and adiabatic control of dipole moments through applied magnetic fields[5,6], all of which unambiguously point to the strong coupling of electric and magnetic degrees of freedom. A number of theories has been advanced to establish a microscopic understanding of these couplings[7–13].

The known mechanisms of the spin-polarization coupling fall into two categories. One is of the inverse Dyzaloshinskii-Moriya (DM) type, whereby the local dipole moment, denoted by u_{ij}, couples to the spins S_i by $\sim u_{ij} \cdot \hat{e}_{ij} \times (S_i \times S_j)$. Here the unit vector $\hat{e}_{ij}$ connects the centers of the magnetic ions at i and j. The microscopic origin of such coupling was investigated in, for instance, Refs. 7,11. The behavior of a large class of multiferroic materials can be understood on the basis of this coupling[1]. The other type arises from exchange-striction, wherein the movement of the magnetic ions is assumed to directly influence the exchange integral and lead to the coupling $\sim \hat{e}_{ij} \cdot (u_i - u_j) S_i \cdot S_j$. The spin-lattice coupling in RMn_2O_5 (R=rare earth) is believed to arise from this mechanism[14].

More recently, the dynamical aspect of the magnetoelectric coupling has been investigated both experimentally[15,16] and theoretically[17]. The dynamical coupling is important because it can arise without the ordering of one or both of the degrees of freedom, and can substantially influence the ac dielectric response[15–17], or even result in an exotic new phase with vector chirality[18]. The dynamics of the small fluctuations in the ordered phase of both the polarization and the spin were examined in Ref. 7 for the one-dimensional frustrated chain. A corresponding analysis of the coupled fluctuations has not yet been tried in the case of the exchange-striction mechanism, or for other lattice geometries.

Triangular geometry offers a potentially fertile ground for the interplay of spin and dipolar degrees of freedom because of the tendency of spins to form a spiral (120°) structure even without further frustrating interactions. The ground state is characterized by non-zero $\langle S_i \cdot S_j \rangle$ as well as $\langle S_i \times S_j \rangle$, which may result in spin-dipole interactions of both DM and exchange-striction types. Furthermore, quite recently, it was shown that a spin $S = 5/2$ triangular antiferromagnet in $RbFe(MoO_4)_2$[19] develops spontaneous polarization along the c axis as the spins order in the ab plane. This and another triangular lattice compound, $YMnO_3$, offer promising examples where the interplay of spin and dipolar degrees of freedom can be revealed in detail. In particular, the dynamical aspect of the spin-dipole coupling in the triangular lattice remains largely unexplored and a theoretical consideration of their interplay would be timely.

In this paper, we examine the coupled dynamics of Heisenberg spins and the local dipolar variable (hereafter referred to simply as phonons) on the triangular lattice, assuming the exchange-striction interaction. In Sec. II, the model Hamiltonian is introduced and solved within Holstein-Primakoff theory. A number of physical quantities, such as the local magnetic moment, phonon correlation function, and the dynamic spin-spin correlation, are derived in Sec. III. Conclusions and the relevance of our work to existing experiments can be found in Sec. IV.

II. SPIN-PHONON MODEL

The spin-phonon coupled Hamiltonian in the exchange-striction picture reads[20]

$$H = \sum_{\langle ij \rangle} [J_0 - J_1 \hat{e}_{ji} \cdot (u_j - u_i)] S_i \cdot S_j + \sum_i \left(\frac{p_i^2}{2m} + \frac{K}{2} u_i^2 \right), \quad (1)$$

where the antiferromagnetic exchange integral J_{ij} connecting the two nearest-neighbor Heisenberg spins is expanded to first order in the displacement u_i of each atomic site i. $\hat{e}_{ji}$ is the unit vector extending from i

to j atomic sites. The terms proportional to J_1 define the spin-phonon coupling. The Heisenberg spin of magnitude S is represented by S_i, and the two-dimensional displacement vectors and their canonical conjugate operators by u_i and p_i. We separate the Hamiltonian into two parts, $H = H_0 + H_1$, where H_1 is the spin-phonon interaction term and H_0 consists of the Heisenberg and phonon Hamiltonians

$$\begin{aligned} H_0 &= J_0 \sum_{\langle ij \rangle} S_i \cdot S_j + \sum_i \Big(\frac{p_i^2}{2m} + \frac{K}{2} u_i^2 \Big), \\ H_1 &= J_1 \sum_{\langle ij \rangle} \hat{e}_{ji} \cdot (u_i - u_j) S_i \cdot S_j. \end{aligned} \tag{2}$$

The classical ground state of the above Hamiltonian was worked out in Ref. 20. It was shown that, despite the spin-phonon coupling term, the classical spin configuration is that of the pure Heisenberg model on the triangular lattice with the neighboring spins at a 120° angle with each other.

Although the spin-phonon interaction does not produce any observable effect in the ground state spin configuration, the excitation spectra of the lattice (phonons) and the spins (magnons) will be mixed due to H_1.

The small fluctuations near the ground state can be analyzed within the standard Holstein-Primakoff (HP) approach after first rotating the spin operators according to their classical spin orientations defined by $\langle S_i \rangle = (0, \sin\phi_i, \cos\phi_i)$, where ϕ_i is the angle the spin makes with the z-axis at site i. All the spins are assumed to lie in the yz-plane, which also coincides with the plane of the lattice itself. After performing the Bogoliubov rotation defined by the angle $\tanh\phi_k = 3\gamma_k/(2+\gamma_k)$ to obtain the spin wave spectrum, the Hamiltonian H_0 reads

$$H_0 = \sum_k \varepsilon_k \alpha_k^\dagger \alpha_k + \omega_0 \sum_k \Big(b_{ky}^\dagger b_{ky} + b_{kz}^\dagger b_{kz} \Big) \tag{3}$$

with the spin wave dispersion

$$\varepsilon_k = \frac{3J_0 S}{2} \sqrt{(1-\gamma_k)(1+2\gamma_k)}. \tag{4}$$

Here $\gamma_k = (1/3)\sum_{\alpha=1}^{3} \cos[k \cdot \hat{e}_\alpha]$ with $\hat{e}_1 = (1,0)$, $\hat{e}_2 = (-1/2, \sqrt{3}/2)$, and $\hat{e}_3 = (-1/2, -\sqrt{3}/2)$. The lattice constant is taken to unity. Phonon operators in the y and z directions are also introduced above as b_{ky} and b_{kz} as well as the phonon energy ω_0.

The spin-phonon Hamiltonian H_1 can be expanded to second order in the magnon and phonon operators. The full spin-phonon Hamiltonian to quadratic order is given in the simple form $(\bar{k} \equiv -k)^{22}$

$$H = \sum_k \Big[\varepsilon_k \alpha_k^\dagger \alpha_k + \omega_0 \beta_k^\dagger \beta_k + i\lambda_k \Big(\alpha_k^\dagger - \alpha_{\bar{k}} \Big) \Big(\beta_k + \beta_{\bar{k}}^\dagger \Big) \Big] \tag{5}$$

where

$$\begin{aligned} \lambda_k &= -\frac{3}{4} J_1 S \sqrt{\frac{S}{m\omega_0}} e^{\frac{\phi_k}{2}} \sqrt{\chi_{ky}^2 + \chi_{kz}^2}, \\ \chi_{ky} &= \cos(k \cdot \hat{e}_3) - \cos(k \cdot \hat{e}_2), \\ \sqrt{3}\chi_{kz} &= 2\cos(k \cdot \hat{e}_1) - \cos(k \cdot \hat{e}_2) - \cos(k \cdot \hat{e}_3). \end{aligned} \tag{6}$$

Note that only the following linear combination of the phonons participate in the interaction with the magnons:

$$\beta_k = \frac{\chi_{ky} b_{ky} + \chi_{kz} b_{kz}}{\sqrt{\chi_{ky}^2 + \chi_{kz}^2}}. \tag{7}$$

The rotation of the Hamiltonian to the diagonalized basis is effected by a series of canonical transformations given by $\psi_k = W_k X_k Y_k \Psi_k$ where Ψ_k, the diagonal operators, are given by $(\mathcal{A}_{1k}, \mathcal{A}_{2\bar{k}}^\dagger, \mathcal{A}_{2k}, \mathcal{A}_{1\bar{k}}^\dagger)^T$. The respective matrices are defined as follows:

$$\begin{aligned}
W_k &= \begin{pmatrix} \cos\frac{\theta_k}{2} & 0 & -i\sin\frac{\theta_k}{2} & 0 \\ 0 & i\sin\frac{\theta_k}{2} & 0 & \cos\frac{\theta_k}{2} \\ -i\sin\frac{\theta_k}{2} & 0 & \cos\frac{\theta_k}{2} & 0 \\ 0 & \cos\frac{\theta_k}{2} & 0 & i\sin\frac{\theta_k}{2} \end{pmatrix}, \quad &&\begin{cases} \sin\theta_k = \frac{2\lambda_k}{\sqrt{(\varepsilon_k-\omega)^2+4\lambda_k^2}} \\ \cos\theta_k = \frac{\varepsilon_k-\omega}{\sqrt{(\varepsilon_k-\omega)^2+4\lambda_k^2}} \end{cases} \\
X_k &= \begin{pmatrix} \cosh\frac{\nu_k}{2} & -i\sinh\frac{\nu_k}{2} & 0 & 0 \\ i\sinh\frac{\nu_k}{2} & \cosh\frac{\nu_k}{2} & 0 & 0 \\ 0 & 0 & \cosh\frac{\nu_k}{2} & -i\sinh\frac{\nu_k}{2} \\ 0 & 0 & i\sinh\frac{\nu_k}{2} & \cosh\frac{\mu_{1k}}{2} \end{pmatrix}, \quad &&\begin{cases} \sinh\nu_k = \frac{\Delta_k}{\sqrt{\Delta_k^2-\Lambda_k^2}} \\ \cosh\nu_k = \frac{\Lambda_k}{\sqrt{\Delta_k^2-\Lambda_k^2}} \end{cases} \\
Y_k &= \begin{pmatrix} \cosh\frac{\mu_{1k}}{2} & 0 & 0 & \sinh\frac{\mu_{1k}}{2} \\ 0 & \cosh\frac{\mu_{2k}}{2} & \sinh\frac{\mu_{2k}}{2} & 0 \\ 0 & \sinh\frac{\mu_{2k}}{2} & \cosh\frac{\mu_{2k}}{2} & 0 \\ \sinh\frac{\mu_{1k}}{2} & 0 & 0 & \cosh\frac{\mu_{1k}}{2} \end{pmatrix}, \quad &&\begin{cases} \sinh\mu_{1k} = \frac{\Gamma_k}{E_{1k}}, \quad \sinh\mu_{2k} = \frac{\Gamma_k}{E_{2k}} \\ \cosh\mu_{1k} = \frac{\mathcal{E}_{1k}}{E_{1k}}, \quad \cosh\mu_{2k} = \frac{\mathcal{E}_{2k}}{E_{2k}} \end{cases}
\end{aligned} \tag{8}$$

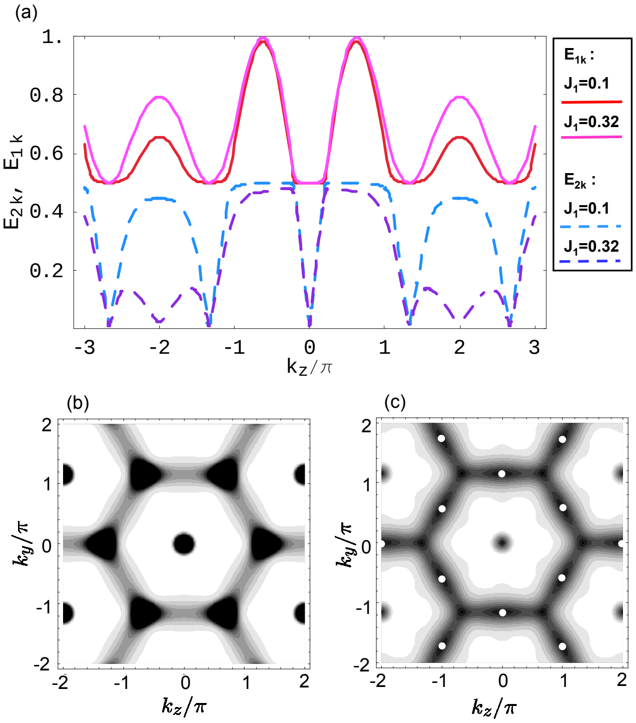

FIG. 1: (color online) (a) Dispersion along the $(k_z, 0)$ direction for E_{1k}(solid) and E_{2k}(dashed) for two choices of spin-phonon coupling, $J_1 = 0.1$ (red and blue lines) and $J_1 = 0.32$ (pink and violet lines). We have chosen $J_0 = 3.7$ to normalize the maximum energy value to one. Other parameters are $S = 1/2$, $\omega_0 = 0.5$, and $m = 2$. The phonon wave function width is chosen $1/\sqrt{m\omega_0} = 1$, equal to the lattice constant. The level repulsion is particularly severe at $(k_z, k_y) = (2\pi, 0)$ as the strength of the coupling is increased. (b)-(c) Contour plots of the low-energy branch E_{2k} for (b) $J_1 = 0.1$ and (c) 0.32. Indicated as white dots in (c) are the k points where E_{2k} reaches zero at the critical spin-phonon coupling.

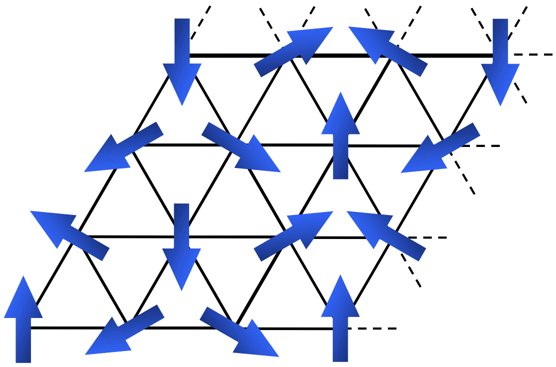

FIG. 2: (color online) The new emergent spin configuration for the critical spin-phonon coupling value $J_1 = J_{1c}$ corresponding to the ordering wave vector $Q' = (4\pi/3 \pm 2\pi, 0)$, or, equivalently, $Q' = \pm(2\pi/3, 0)$. This configuration becomes degenerate with those at $Q = \pm(4\pi/3, 0)$ when J_1 equals J_{1c}.

where $\Lambda_k = \lambda_k \cos\theta_k$, $\Gamma_k = \lambda_k \sin\theta_k$, $\Delta_k = \frac{\Delta_{1k}+\Delta_{2k}}{2}$, $\delta_k = \frac{\Delta_{1k}-\Delta_{2k}}{2}$, $\mathcal{E}_{1k,2k} = \sqrt{\Delta_k^2 - \Lambda_k^2} \pm \delta_k$, $E_{1k,2k} = \sqrt{\mathcal{E}_{1k,2k}^2 - \Gamma_k^2}$, and $\Delta_{1k,2k} = \frac{\varepsilon_k+\omega}{2} \pm \frac{1}{2}\sqrt{(\varepsilon_k-\omega)^2 + 4\lambda_k^2}$. The final form of the Hamiltonian is

$$\begin{aligned} Y_k^\dagger X_k^\dagger W_k^\dagger \mathcal{H}_k W_k X_k Y_k &= \mathrm{diag}(E_{1k}, E_{2k}, E_{2k}, E_{1k}) \\ H &= \sum_k \left(E_{1k}\mathcal{A}_{1k}^\dagger \mathcal{A}_{1k} + E_{2k}\mathcal{A}_{2k}^\dagger \mathcal{A}_{2k} \right). \end{aligned} \tag{9}$$

The sum $\sum_k$ is over the entire Brillouin zone. For any given k we have $E_{1k} \geq E_{2k}$, constituting an upper and lower branch of the spectra.

A plot of E_{1k} and E_{2k} in Fig. 1 shows the change in the magnon and the phonon spectrum as J_1 is increased. The most notable feature in the coupled energy spectrum is the appearance of the roton-like minimum at a set of k-points in the Brillouin zone. When J_1 equals the threshold value, *e.g.* $J_{1c} \equiv 0.321$ for $S = 1/2$, $\omega_0 = 0.5$, and the phonon wave function width $m\omega_0 = 1$, E_{2k} touches zero at $k = (2\pi, 0)$, $(0, 2\pi/\sqrt{3})$, and all their sixfold symmetry-related points indicated as white dots in Fig. 1 (c). The original zeros of the magnon spectrum at $\pm(4\pi/3, 0)$ remain intact through nonzero J_1.

As this happens, one has a new spin-ordered pattern illustrated in Fig. 2 becoming degenerate with the original 120° ordered phase. This new pattern is obtained by rotating spins counterclockwise by 120° along the $\hat{e}_1$ direction and by 60°, also counterclockwise, along the $\hat{e}_2$ direction. The state where the spins are rotated clockwise in both directions will also be degenerate, carrying the opposite sense of chirality. In terms of ordering wave vectors, the new ground states are characterized by $Q' = \pm(2\pi/3, 0)$ instead of $Q = \pm(4\pi/3, 0)$ as in the 120° ordered phase.

III. PHYSICAL QUANTITIES

The local staggered magnetization (uniform magnetization in the rotated basis), $\langle \boldsymbol{S} \rangle \equiv (1/N)\sum_i \langle \boldsymbol{S}_i^z \rangle$, is modified due to the spin-phonon coupling. The quantum correction, defined as the difference of the classical and quantum averages $S - \langle \boldsymbol{S} \rangle$, reads

$$\sum_k \left(\sinh^2\frac{\phi_k}{2} + \cosh\phi_k \langle \alpha_k^\dagger \alpha_k \rangle - \sinh\phi_k \langle \alpha_k^\dagger \alpha_k^\dagger \rangle \right), \tag{10}$$

which is plotted at $T = 0$ in Fig. 3 for various spin values as the coupling strength is varied. In small powers of λ_k one obtains the following perturbative expression as the quantum correction

$$\sum_k \sinh^2\frac{\phi_k}{2} + \sum_k \frac{\lambda_k^2 \cosh\phi_k}{(\varepsilon_k + \omega_0)^2} + \sum_k \frac{\lambda_k^2 \sinh\phi_k}{\varepsilon_k(\varepsilon_k + \omega_0)}. \tag{11}$$

The first term is the usual quantum fluctuation correction, and the latter two account for further corrections due to spin-phonon coupling. There is only a tiny change in the local magnetization affected by the spin-phonon coupling. On the other hand, the upturn found in Fig. 3 as J_1 is driven up to its critical value is probably indicative of the diverging quantum correction as the new ground state is approached. Due to the finite phonon mass ω_0, the spin-phonon coupling effects are not apparent until very near the criticality.

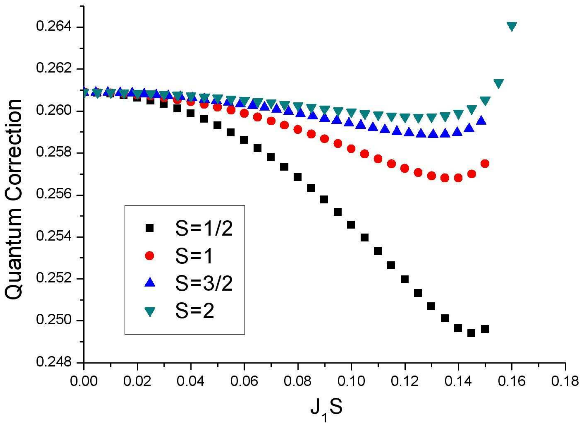

FIG. 3: (color online) Plot of the quantum correction versus the coupling strength for various spin values and $0 < J_1S < J_{1c}S$. The critical coupling strength depends on S, while the product J_1S is nearly independent of S. Choices of other parameters are the same as in Fig. 1.

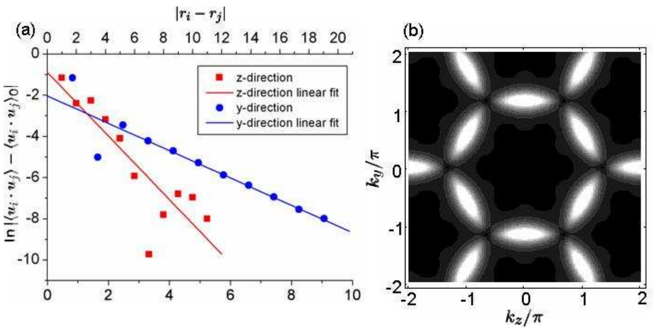

FIG. 4: (color online) (a) Log plots of the correlation function $|\langle \boldsymbol{u}_i \cdot \boldsymbol{u}_j\rangle - \langle \boldsymbol{u}_i \cdot \boldsymbol{u}_j\rangle_0|$ in the z and y directions. Using the same parameter values as in Fig. 1, the correlation length can be extracted as ~ 1.36 and ~ 3.16 lattice constants in the z and y directions, respectively. (b) Plot of $G_k - 1$. Bright regions indicate peaks in $G_k - 1$.

The equal-time phonon correlation function $\langle \mathbf{u}_i \cdot \mathbf{u}_j\rangle$, which will be short-ranged $\langle \mathbf{u}_i \cdot \mathbf{u}_j\rangle_0 = \delta_{ij}$ (since we have chosen $m\omega_0 = 1$) in the absence of spin-phonon coupling, now reads

$$\langle \mathbf{u}_i \cdot \mathbf{u}_j\rangle - \langle \mathbf{u}_i \cdot \mathbf{u}_j\rangle_0 = \frac{\sqrt{3}}{16\pi^2}\int_{\mathrm{BZ}} e^{ik\cdot(r_i - r_j)}(G_k - 1)d^2k,$$
$$G_k = \langle(\beta_k + \beta^\dagger_{\bar{k}})(\beta^\dagger_k + \beta_{\bar{k}})\rangle, \tag{12}$$

at zero temperature. A log plot of $|\langle \mathbf{u}_i \cdot \mathbf{u}_j\rangle - \langle \mathbf{u}_i \cdot \mathbf{u}_j\rangle_0|$ is given in Fig. 4, showing an exponential decay with a correlation length which depends on the parameters. The momentum space correlation G_k shows pronounced peaks around $k = (0, 2\pi/\sqrt{3})$ and other symmetry-related points as shown in Fig. 4 (b). These are the same points where E_{2k} shows pronounced minima for large J_1. Detection of such peaks in the phonon structure factor G_k will be instrumental in identifying the spin-phonon coupling in a triangular antiferromagnet.

The spin-spin correlation function, $\langle S^+_j(t)S^-_i(0)\rangle$, can be an effective probe of the spin-phonon coupling. Using the straightforward algebra we have calculated the absorption spectra $I(k,\omega)$ as the imaginary part of the Fourier transform of the spin-spin correlation function,

$$\begin{aligned} I(k,\omega) = \frac{\pi S}{8}\Bigg[&\sum_{\alpha=1,2} e^{\phi_{k_\alpha}}\Big((B_{1k_\alpha} - A_{1k_\alpha})\delta(\omega - E_{1k_\alpha}) + (B_{2k_\alpha} - A_{2k_\alpha})\delta(\omega - E_{2k_\alpha})\Big) \\ &+ 2e^{-\phi_k}\Big((A_{1k} + B_{1k})\delta(\omega - E_{1k}) + (A_{2k} + B_{2k})\delta(\omega - E_{2k})\Big)\Bigg], \end{aligned} \tag{13}$$

which is plotted in Fig. 5. The functions appearing in Eq. (13) are defined as $k_{1,2} = k \pm (4\pi/3, 0)$, and

$$\begin{aligned} A_{1k} &= \sinh\mu_{1k}(\cos\theta_k + \cosh\nu_k) - \cosh\mu_{1k}\sin\theta_k\sinh\nu_k \\ A_{2k} &= \sinh\mu_{2k}(\cos\theta_k - \cosh\nu_k) - \cosh\mu_{2k}\sin\theta_k\sinh\nu_k \\ B_{1k} &= \cosh\mu_{1k}(\cos\theta_k + \cosh\nu_k) - \sinh\mu_{1k}\sin\theta_k\sinh\nu_k \\ B_{2k} &= \cosh\mu_{2k}(\cosh\nu_k - \cos\theta_k) + \sinh\mu_{2k}\sin\theta_k\sinh\nu_k. \end{aligned} \tag{14}$$

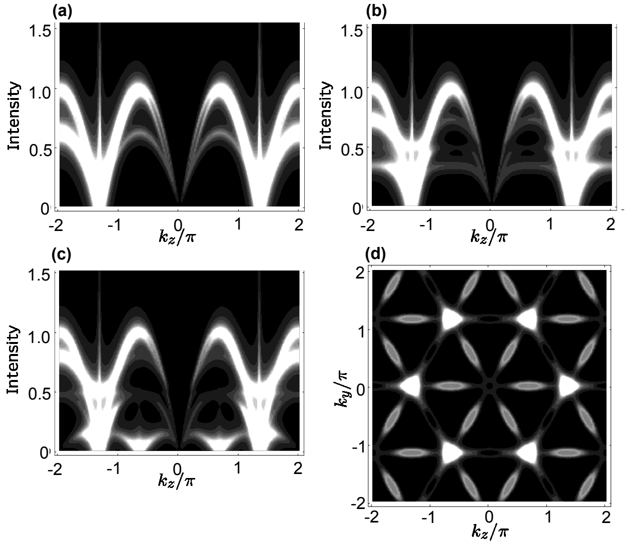

FIG. 5: Plots of the spectral function $I(k, \omega)$ along the k_z-direction ($k_y = 0$) for (a) $J_1 = 0$, (b) $J_1 = 0.2$, and (c) $J_1 = 0.32$. Emergence of a new low-energy feature at $k_z = 2\pi/3$ for J_1 close to the critical value $J_{1c} = 0.321$ is apparent in (c). (d) Plot of $I(k_z, k_y, \omega = 0.1)$ clearly indicates new intensity peaks at $(2\pi/3, 0)$ and other symmetry points (elongated and shaded) while the bright patterns at $(4\pi/3, 0)$ and etc. are due to the original spin waves.

The flattening and the eventual collapse of the excitation band found earlier now manifests itself as intensity patterns at $(k_z, k_y) = (2\pi/3, 0)$ and its rotational counterparts as can be seen in Fig. 5 (d).

IV. DISCUSSION

In summary, we have considered the magnon-phonon coupling in the exchange-striction coupled triangular lattice antiferromagnet for Heisenberg spins in the Holstein-Primakoff approach. The dynamics of the lattice and the spins are coupled to produce interesting modifications in the excitation spectra, in particular (i) the significant lowering of the magnon excitation energy at wave vector transfer $\pm 2\pi$ as indicated in Fig. 1, and (ii) the concordant variation in the phonon structure factor as shown in Fig. 4 (b). Detection of an additional low-energy spectra in the spin spectral function $I(k, \omega)$ and in the phonon structure factor G_k through neutron scattering experiments will be a clear hint of the strong spin-phonon coupling.

Naively speaking, integrating out the phonon coordinate from Eq. (1) would generate the effective interaction, $\sim -\sum_i (\sum_{j=\text{NN of } i} \hat{e}_{ij} S_i \cdot S_j)^2$, which embodies the ferromagnetic biquadratic exchange, $-(S_i \cdot S_j)^2$, and some three-body interactions as well. A quantum spin model involving quadratic and biquadratic exchanges were considered extensively[23] following the discovery of the liquid-like ground state in the triangular antiferromagnet NiGa_2S_4[24]. The ground state revealed correlations, dynamic on the scale of ~ 1 ns, of a period-six spin orientation (60° angles between nearest neighbors), quite unlike the period-three orientation (120° angles between nearest neighbors) expected in the triangular lattice. It is not easy to reproduce such a spin structure in the mean field solution of the spin models considered in Refs. 23. In fact, the spin-spin correlation observed in NiGa_2S_4 is almost exactly the one shown in Fig. 2. To correctly account for the observed periodicity of spins in NiGa_2S_4, one would have to consider an extended-neighbor interaction as in Ref. 25, or some dynamical consequence of spin-phonon coupling as in the present paper.

We wish to acknowledge fruitful discussions with Chenglong Jia. Discussions with Satoru Nakatsuji on NiGa_2S_4 are also gratefully acknowledged. H. J. H. was partly supported by the Samsung Research Fund, Sungkyunkwan University, 2006.

---

[*] Electronic address: `hanjh@skku.edu`

[1] A recent review of the subject can be found in Y. Tokura, Science **312**, 1481 (2006); Sang-Wook Cheong and Maxim Mostovoy, Nature Materials **6**, 13 (2007).

[2] G. Lawes *et al.*, Phys. Rev. Lett. **95**, 087205 (2005).

[3] M. Kenzelmann *et al.*, Phys. Rev. Lett. **95**, 087206 (2005).

[4] Seongsu Lee *et al.*, Phys. Rev. B **71**, 180413 (2005).

[5] T. Kimura, T. Goto, H. Shintani, K. Ishizaka, T. Arima, and Y. Tokura, Nature **426**, 55 (2003).

[6] N. Hur, S. Park, P. A. Sharma, J. S. Ahn, S. Guha, and S.-W. Cheong, Nature **429**, 392 (2004).

[7] Hosho Katsura, Naoto Nagaosa, and Alexander V. Balatsky, Phys. Rev. Lett. **95**, 057205 (2006).

[8] Maxim Mostovoy, Phys. Rev. Lett. **96**, 067601 (2006).

[9] I. A. Sergienko and E. Dagotto, Phys. Rev. B **73**, 094434 (2006).

[10] A. B. Harris, T. Yildirim, A. Aharony, and O. Entin-Wohlman, Phys. Rev. B **73**, 184433 (2006).

[11] Chenglong Jia, Shigeki Onoda, Naoto Nagaosa, and Jung Hoon Han, Phys. Rev. B **74**, 224444 (2006); cond-mat/0701614.

[12] Bas B. van Aken, Thomas T. M. Palstra, Alessio Filippetti, and Nicola A. Spaldin, Nature Materials **3**, 164 (2004).

[13] Chenglong Jia and Jung Hoon Han, Phys. Rev. B **73**, 172411 (2006).

[14] L. C. Chapon *et al.* Phys. Rev. Lett. **93**, 177402 (2004); L. C. Chapon *et al.* Phys. Rev. Lett. **96**, 097601 (2006).

[15] A. Pimenov *et al.*, Nature Physics **2**, 97 (2006).

[16] A. B. Sushkov *et al.*, Phys. Rev. Lett. **98**, 027202 (2007).

[17] Hosho Katsura, Alexander V. Balatsky, and Naoto Nagaosa, Phys. Rev. Lett. **98**, 027203 (2007).

[18] Shigeki Onoda and Naoto Nagaosa, cond-mat/0703064.

[19] M. Kenzelman *et al.* arXiv:cond-mat/0701426 [cond-mat.mtrl-sci].

[20] Chenglong Jia, Jung Ho Nam, June Seo Kim, and Jung Hoon Han, Phys. Rev. B **71**, 212406 (2005).

[21] Ann Mattsson, Phys. Rev. B **51**, 11574 (1995).

[22] In the unrotated spin basis the phonon at momentum k couples to the magnon at $k \pm Q$, where Q is the ordering wave vector $(4\pi/3, 0)$. Due to the rotation that aligns the spins ferromagnetically, the magnon-phonon coupling appears between the same k states.

[23] Hirokazu Tsunetsugu and Mitsuhiro Arikawa, J. Phys. Soc. Jpn. **75**, 083701 (2006); Andreas Läuchli, Frédéric Mila, and Karlo Penc, Phys. Rev. Lett. **97**, 087205 (2006); Subhro Bhattacharjee, Vijay B. Shenoy, and T. Senthil, Phys. Rev. B **74**, 092406 (2006).

[24] Satoru Nakatsuji *et al.* Science **309**, 1697 (2005).

[25] K. Takubo *et al.* arXiv:0706.2217 [cond-mat.str-el]; To appear in Phys. Rev. Lett.